Heliyon 10 (2024) e30233

Contents lists available at ScienceDirect

Heliyon

journal homepage: www.cell.com/heliyon

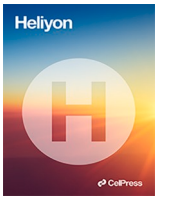

Research article

Synergistic effects and competitive relationships between DOC and DOX as acting on DNA molecules: Studied with confocal Raman spectroscopy and molecular docking technology

Suli Zhou [a], Xiaoqiang Feng [a], Jintao Bai [a], Dan Sun [a], Baoli Yao [b], Kaige Wang [a,*]

[a] Key Laboratory of Photoelectronic Technology of Shaanxi Province, National Center for International Research of Photoelectric Technology & Nano-Functional Materials and Application, Institute of Photonics and Photon-Technology, Northwest University, Xi'an, 710127, China
[b] State Key Laboratory of Transient Optics and Photonics, Xi'an Institute of Optics and Precision Mechanics, Chinese Academy of Sciences, Xi'an, 710119, China

ARTICLE INFO

Keywords:
Laser confocal Raman spectroscopy
Docetaxel
Drug-DNA interaction
Synergistic and competitive effects
Molecular docking

ABSTRACT

Docetaxel (DOC) is one of the second-generation antineoplastic drugs of the taxanes family with excellent antitumor activity. However, the mechanism of DOC inducing tumor cell apoptosis and treating cancer diseases, especially its interaction with DNA in the nucleus, and its adjuvant or combined Doxorubicin (DOX) acting on DNA molecules are unclear. In this study, the interaction mechanism between DOC and DNA, as well as the synergistic effects and competitive relationships among DOC and DOX when they simultaneously interact with DNA molecules were studied by laser confocal Raman spectroscopy combined with UV–visible absorption spectroscopy and molecular docking technology. The spectroscopic results showed that the binding constant of DOC to DNA is 5.25×10^3 M^{-1}, the binding modes of DOC and DNA are non-classical intercalation and electrostatic binding, and the DNA-DOC complex has good stability. When DOC or DOX interacts with DNA alone, both of them can bind with bases and phosphate backbone of DNA, and also lead to DNA conformation changes; when DOC and DOX interact with DNA at the same time, the orders of interaction not only affect their binding sites with DNA, but also cause changes in the surrounding environment of the binding sites. In addition, the molecular docking results further verified that DOC and DOX have synergy and competition when they interact with DNA molecules simultaneously. The docking energies of DNA-DOC and DNA-DOX indicate the important role of van der Waals forces and hydrogen bonds. This study has practical significance for the design and development of antitumor drugs with less toxic based on the taxanes family and the combination with other drugs for the treatment of cancer.

1. Introduction

DNA (Deoxyribonucleic Acid) is a crucial genetic material in organisms and is also the target of drugs [1]. Many anticancer drugs used in clinical therapy exert their biological effects by interfering with the transcription and replication of DNA. The binding modes between drugs and DNA are closely associated with the chemical structure, molecular conformation and the distribution of extranuclear electron clouds of drug molecules, the modes can be simply classified into covalent, non-covalent and cleavage interactions [2,

* Corresponding author.
E-mail address: wangkg@nwu.edu.cn (K. Wang).

https://doi.org/10.1016/j.heliyon.2024.e30233
Received 3 March 2024; Received in revised form 10 April 2024; Accepted 22 April 2024
Available online 23 April 2024

3]. Non-covalent binding involves electrostatic, groove and intercalative binding [4,5]. When small drug molecules interact with DNA, it can be a singular mode or multiple modes coexisted. It is a basis that exploring the interaction mechanism between drug molecules and DNA for understanding the mechanism of drug-induced apoptosis of tumor cells and developing new drugs with less toxicity.

Docetaxel (DOC) is one of the second-generation anticancer drugs of taxanes family and a semisynthetic analogue of 10-deacetyl-baccatin-III derived from the needles of yew tree Taxus baccata [6]. DOC has some excellent properties such as better water solubility than paclitaxel due to its chemical structure containing tert-butyl carbamate in the phenylpropionate side chain and a hydroxyl group at C10, as well as lower toxicity and higher efficacy in anticancer activity. Recently, DOC has been attracted more and more attention [7].

DOC can stabilize microtubules through binding to tubulin and inhibit its depolymerization, resulting in cell cycle arrest at G2/M phase and inhibiting the proliferation and viability of cancer cells. Additionally, DOC can promote the expression of the cell cycle inhibitor p27 while inhibit the expression of anti-apoptotic gene Bcl-2 [8]. DOC has remarkable efficacy and tolerability in clinical applications, showing excellent antitumor activity in various cancers such as breast cancer, pancreatic cancer and non-small cell carcinomas [9].

Studying and analyzing the interaction between small drug molecules and DNA can help deeply comprehend the pharmacological activity of drugs. At present, the main methods and technologies include ultraviolet visible spectroscopy (UV–vis) [10], fluorescence spectroscopy [11], isothermal titration calorimetry (ITC) [12], magnetic tweezer [13], optical tweezers [14], Atomic Force Microscope (AFM) [15] and so on. However, these methods have limitations of some sort. Laser confocal Raman spectroscopy overcomes the shortcomings of low sensitivity and weak spectral intensity of ordinary Raman spectroscopy and has many advantages such as high accuracy and efficiency in the detection of single molecular characteristics [16,17].

Rezaei et al. have evaluated the binding mechanism of Piperine and calf thymus DNA and confirmed the groove binding of Piperine to DNA [18]. Esfandiari et al. have investigated the interaction of Rebeccamycin with calf thymus DNA in the absence and presence of H1 by molecular dynamics and multi-spectroscopic. The results showed that Rebeccamycin can interact with DNA by intercalation and groove binding in the absence and presence of H1 [19]. Sani et al. have studied the interaction of Ofloxacin (Oflx) and calf thymus DNA in the presence and absence of histone H1 by multi-spectroscopic. The results indicated that the interaction mode between Oflx and DNA is intercalation binding, and the binding of Oflx to DNA-H1 complex is mainly driven by hydrogen bonding and van der Waals forces [20].

In clinical applications and exploratory developments, it is found that adjuvant and combination chemotherapy can achieve synergistic therapeutic effect to improve anticancer efficacy and reduce side effects [21]. Among them, the combination of DOC and DOX has gained attention in the treatment of breast cancer, ovarian cancer and other cancers [22–24]. Doxorubicin (DOX) is a broad-spectrum anthracycline derived from mutated strains of streptomyces peucetius [25]. DOX prevents the proliferation of cancer cells by inserting base pairs to interrupt DNA transcription and inhibit the activity of topoisomerase II to impede DNA replication [26]. DOX has remarkable therapeutic efficacy on various cancers such as acute leukemia, breast cancer and multiple myeloma [27].

Lemiesz et al. have investigated the binding between taxane and human serum albumin and the influence of taxane on the interaction between DOX and serum albumin by spectroscopic methods. It was found that the binding of taxane to serum albumin can occur near the binding sites of DOX to serum albumin, and can induce surrounding conformation changes of serum albumin [28]. Chen et al. have found that taxane can significantly enhance the resonance light scattering (RLS) signal and improve the binding ability of anthracyclines to DNA using RLS technique [29]. Zeng et al. have demonstrated that DOX can interfere with the cytotoxic effect of DOC on both mitotic arrest and apoptotic cell death through DNA fragmentation analyses, flow cytometry and cell rotation analysis [30]. Despite these studies providing partial hypotheses and explanations for the combined effects of taxanes and anthracyclines, further experimental research and theoretical analysis are necessary to elucidate the interaction mechanism between DOC and DNA, as well as the synergistic effects and competitive relationships when DOC and DOX interact with DNA molecules.

In this study, we have investigated the interaction mechanism between DOC and DNA, as well as the synergistic effects and competitive relationships when DOC and DOX interact with DNA molecules simultaneously based on laser confocal Raman spectroscopy, combined with UV–vis spectroscopy. And the molecular docking technology is employed to validated the binding modes and the binding sites between drugs and DNA.

2. Material and methods

2.1. Chemicals and reagents

DOC (CAS: 114977-28-5), DOX (CAS: 23214-92-8) and calf thymus DNA (CAS: 73049-39-5) were purchased from Sigma-Aldrich (St. Louis, Missouri, USA). The stock solution of DOC (1.2×10^{-2} M) was prepared in ethanol, the stock solution of DOX (1.2×10^{-2} M) and DNA (1.5×10^{-3} M) were prepared in Tris-HCL buffer (10 mM, PH = 7.4). All solutions were stored at 4 °C away from light. The concentration of DNA was determined by the molar absorption coefficient $\varepsilon_{260} = 6600$L/(mol•cm) at 260 nm. The purity of DNA was determined by measuring the absorbance ratio at 260/280 nm, $A_{260/280} = 1.9$, indicating its high purity without proteins. All other chemicals and reagents used were of analytical grade.

2.2. Experimental methods

2.2.1. Raman spectroscopy

The Raman spectra of the samples were collected using Alpha 500R laser confocal Raman system, with a 20 × objective lens, a

grating of 600 g/mm. The integration time was 30 s with 2 accumulations per measurement and the range was 400–1800 cm^{-1}. The data were preprocessed using WITec Project Four software, including cosmic ray removal, smoothing, baseline correction and so on. The processed data were exported and the Raman spectra were plotted by Origin. The Raman spectra of DNA, DOC and DOX were characterized and the Raman spectra of binary and ternary system complexes were measured. Five sets of valid data were taken for each experimental group and averaged to obtain the final Raman spectra.

2.2.2. UV–vis spectroscopy

UV–vis spectroscopy enables qualitative, quantitative and structural analysis of molecules by analyzing the position and the absorbance of the peaks [31]. The UV–vis spectra of the samples were collected using the ultramicro UV–vis spectrophotometer (DS-11, DeNovix, USA) to study the effects of different conditions (pH, DNA concentration, interaction time and ionic strength) on the samples. Each set of samples was mixed thoroughly and left at room temperature for half an hour. In the melting point experiment, the UV–Vis spectra of DNA and DNA-DOC were measured at intervals of 5 °C in the range of 20–100 °C and the absorbance at 260 nm was recorded. To ensure the accuracy and reliability of the experimental results, three measurements of each spectrum were averaged and then plotted and analyzed.

2.2.3. Molecular docking method

Molecular docking technology provides valuable information on potential binding modes and interactions between drugs and DNA at the molecular level [32,33]. Molecular docking software Autodock (Scripps, USA) has been used to simulate and calculate all possible binding conformations and interaction forces. After the ligand and receptor were treated with dehydrating and hydrogenation, the grid point position was 70 × 80 × 90 and the grid point spacing was 0.375 Å. Based on Lamarck genetic algorithm, the semi-flexible docking method was used to calculate the docking calculation of receptor and ligand. The optimal binding conformation was selected from the final docking results, and PyMol 2.5.3 software was used to visualize and analyze the docking results. The 3D crystal structure of DNA was downloaded from Protein Data Bank. The structures of DOC and DOX were downloaded from ChemSpider (ChemSpider ID: 130581) and PubChem database (PubChem CID: 31703).

3. Results and discussion

3.1. Raman spectra

3.1.1. Raman spectra of DNA

In order to avoid the variation of DNA Raman peak positions due to different DNA states, Raman spectra of DNA fiber and DNA solution were studied. Fig. 1 shows the Raman spectra of DNA fiber and solution. The main Raman peaks of DNA solution include 733, 785, 807, 838, 1013, 1100, 1250, 1307, 1378, 1423, 1487, 1577, and 1662 cm^{-1}. These characteristic peaks reveal the vibrational information of the DNA molecular structure [34,35]. The 785 cm^{-1} peak represents the symmetric stretching vibration of bases C, T and O–P–O. The 807 cm^{-1} is attributed to A-DNA, while the 838 cm^{-1} is attributed to B-DNA. The 1013 cm^{-1} is attributed to the C–O stretching vibration of deoxyribose and 1100 cm^{-1} corresponds to the O═P═O symmetric stretching vibration. 733, 1250, 1307,

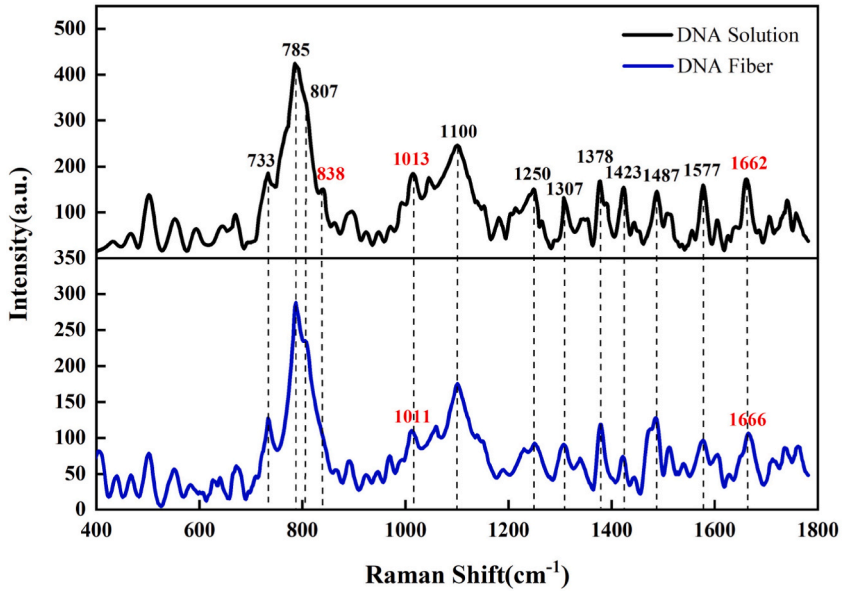

Fig. 1. Raman spectra of DNA fiber and solution, c(DNA) = 1.2 × 10^{-2} M.

1378, 1423, 1487, 1577, and 1662 cm^{-1} are attributed to the relevant vibrations of bases. 733 and 1307 cm^{-1} correspond to the symmetric stretching vibration of base A and 1250 cm^{-1} peak represents the vibrational mode of bases A and C. 1378 cm^{-1} corresponds to the molecular vibration of the three bases A, T and G. 1423 cm^{-1} belongs to the molecular vibration of bases A and G. Both 1487 and 1577 cm^{-1} can be attributed to the molecular vibrations of bases G and A. 1662 cm^{-1} is attributed to the stretching vibration of C═O.

By comparing the Raman spectra of DNA fiber and solution, it is observed that the peak positions are almost the same, with a few peaks being slightly shifted. A new peak of 838 cm^{-1} appeared in the spectra of DNA fiber formulated into solution. At this time, the Raman peaks of 807 and 838 cm^{-1} were found in the DNA solution, indicating that the solution was in the coexistence state of A-DNA and B-DNA [36]. The Raman peaks at 1011 and 1666 cm^{-1} shifted to 1013 and 1662 cm^{-1} respectively. The difference between DNA fiber and DNA solution is that the DNA in solution may be affected by the solvent, which may cause slight changes in DNA conformation and skeleton due to ionic binding or hydration, and thus affect the DNA Raman peak positions [37].

3.1.2. Raman spectra of DOC

The molecular structure of DOC (Fig. 2a) and corresponding Raman spectra (Fig. 2b) are shown in Fig. 2. The main Raman peaks of DOC are concentrated in the range of 600–1800 cm^{-1}, which mainly contains 620, 696, 805, 894, 952, 1002, 1163, 1254, 1274, 1325, 1372, 1455, 1602, 1630 and 1717 cm^{-1}. The Raman peaks at different positions can reveal vibrational information of the DOC molecular structure [38,39]. 620 and 696 cm^{-1} are attributed to the stretching vibration of C═C. 805 cm^{-1} characterized the deformation vibration of C–H. 894 and 952 cm^{-1} belong to the methyl rocking vibration. 1002 and 1163 cm^{-1} are associated with C═C vibration mode. 1254 cm^{-1} is attributed to the stretching vibration of C–C, while 1274 cm^{-1} is attributed to the deformation vibration of carbon alkyl. 1325, 1372 and 1455 cm^{-1} are attributed to the deformation vibration of C–H including CH_2 and CH_3. 1602 cm^{-1} represents the structure of ester and 1630 cm^{-1} represents the stretching vibration of C═C conjugated with C═O. 1717 cm^{-1} represents the stretching vibration of C═O.

3.1.3. Raman spectra of DNA-DOC

Fig. 3 illustrates the Raman spectra of DNA and DNA-DOC. It can be found that when DOC interacted with DNA, the Raman peak at 733 and 1307 cm^{-1} shifted to 740 and 1315 cm^{-1} respectively, indicating a certain interaction between DOC and base A. The Raman peak at 838 cm^{-1} shifted to 845 cm^{-1} indicating that DOC can affect the B conformation of DNA. The Raman peak of 1100 cm^{-1}, attributed to the symmetric stretching vibration of O═P═O, shifted to a lower wave number of 1085 cm^{-1}, due to the hydrogen bond between DOC and the phosphate backbone of DNA. The blueshift of the characteristic peak from 1378 to 1382 cm^{-1} is caused by the deformation of hydrogen bond between the $–NH_2$ of base A and the C═O of base T. The characteristic peak of 1577 cm^{-1} shifted to 1582 cm^{-1}, indicating that DOC molecule can form hydrogen bond with base G. The redshift from 1662 to 1658 cm^{-1} is due to the C═O change of base C. Therefore, DOC can interact with the bases of DNA as well as the phosphate backbone, and can also induce the conformation changes of DNA.

3.1.4. Raman spectra of DOX

The molecular structure of DOX (Fig. 4a) and its corresponding Raman spectra (Fig. 4b) are shown in Fig. 4. The main Raman characteristic peaks of DOX include 440, 463, 792, 992, 1083, 1210, 1245, 1428, 1448, 1578 and 1635 cm^{-1}, which reveal the structural information of DOX [40–42]. The Raman peaks at 440 and 463 cm^{-1} are attributed to C–C–O and C–O vibrations, respectively. 792 cm^{-1} is attributed to the deformation vibration of C–H on the ring, while 992 cm^{-1} is attributed to C–H_2 and the deformation vibration of C═O and C–O-H. 1083 cm^{-1} is assigned to C–O vibration, while 1210 and 1245 cm^{-1} are attributed to C–O–H and C–H vibrations respectively. 1428 cm^{-1} is attributed to vibrations of single and double bonded oxygen on the ring. 1448 cm^{-1} is attributed to ring breathing vibrations and N–H deformation vibration. 1578 cm^{-1} is attributed to ring breathing vibrations. 1635 cm^{-1} is attributed to the stretching vibration of C═O. The Raman spectra of DOX powder was also measured, and the peak of DOX

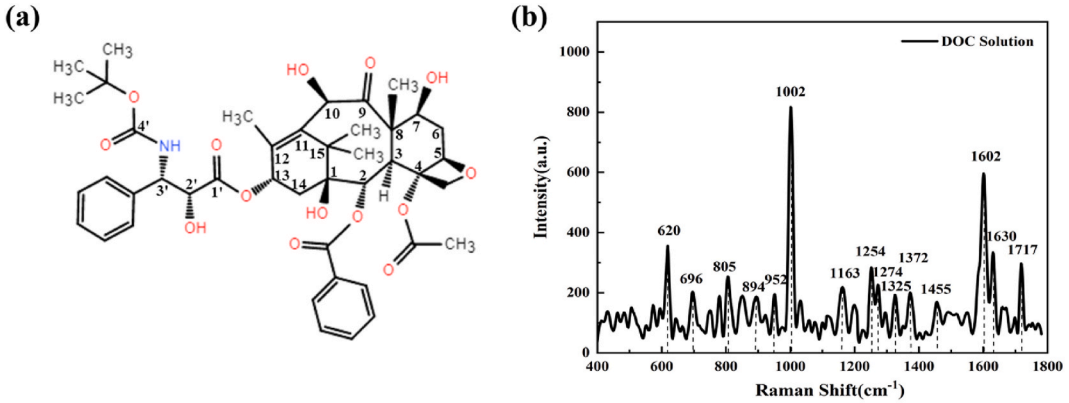

Fig. 2. (a) Molecular structure of DOC; (b) Raman spectra of DOC, c(DOC) = 1.2×10^{-2} M.

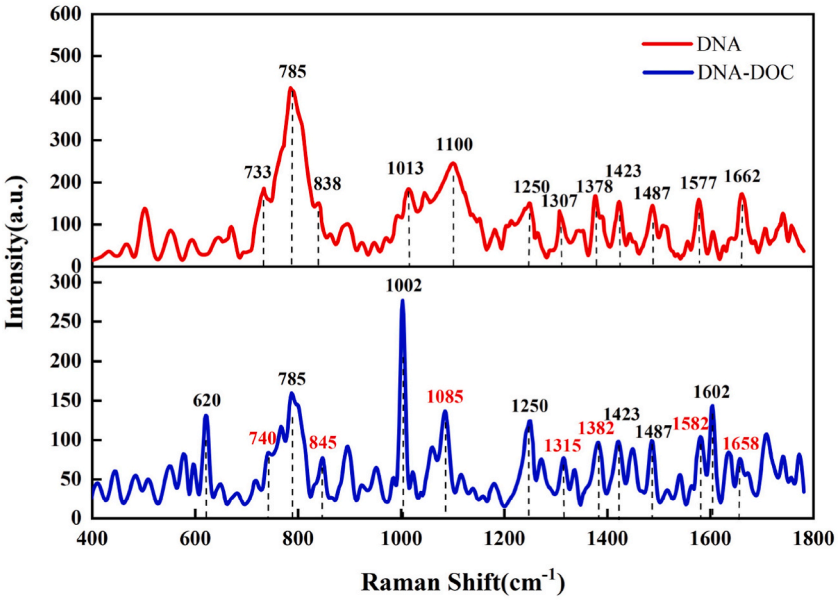

Fig. 3. Raman spectra of DNA and DNA-DOC solution.

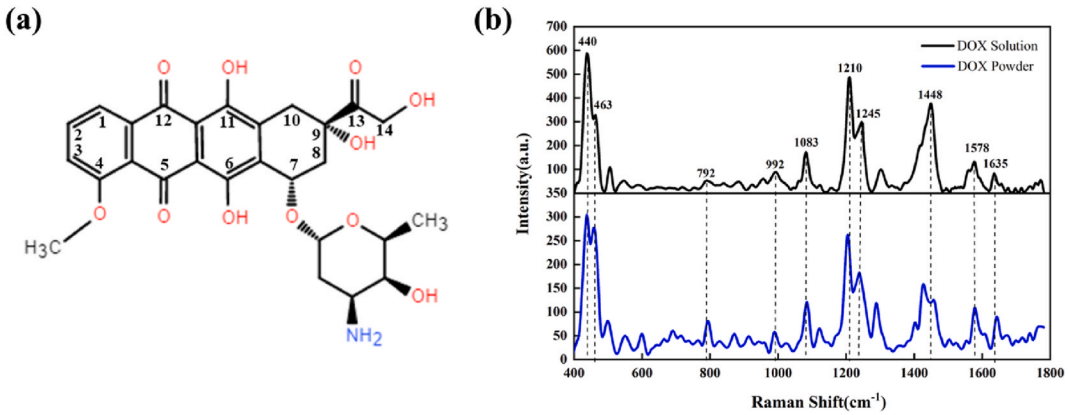

Fig. 4. (a) Molecular structure of DOX; (b) Raman spectra of DOX powder and solution, c(DOX) = 1.2×10^{-2} M.

powder is similar to that of solution, with only a slight shift of 1448 cm^{-1}.

3.1.5. Raman spectra of DNA-DOX

Fig. 5 illustrates the Raman spectra of DNA and DNA-DOX. It can be found that when DOX interacted with DNA, the Raman peak at 733 and 1307 cm^{-1} shifted to 748 and 1312 cm^{-1} respectively, which may be due to the formation of hydrogen bond between DOX and base A. The Raman peak at 838 cm^{-1} shifted to 856 cm^{-1}, indicating the insertion of DOX can affect the B conformation of DNA [43]. The peak of 1100 cm^{-1} shifted to a lower wave number of 1089 cm^{-1}, which is due to the hydrogen bonds between the $-^{NH}_{2}$ and the −OH of DOX with the phosphate backbone of DNA. The blueshift from 1378 to 1384 cm^{-1} is caused by the deformation of the hydrogen bond between the $-NH_2$ of base A and the C═O of base T. 1487 cm^{-1} is sensitive to environmental changes of base G [44], and its blueshift to 1492 cm^{-1} is due to the interaction of DOX with base G [45]. The redshift from 1662 to 1656 cm^{-1} is caused by the formation of hydrogen bond between $–NH_2$ of amino sugar group and the C═O of base C. It can be seen that DOX can not only interact with the adenine, thymine, guanine, cytosine and phosphate backbone of DNA, but also affect the conformation of DNA.

3.1.6. Raman spectra of DNA、DOC and DOX complexes

In order to deeply investigate the interaction mechanism of DNA, DOC and DOX and their mutual influence effects, Raman spectra of DNA, DOC and DOX in different interaction sequences were compared and analyzed, as depict in Fig. 6. Fig. 6a represents the Raman spectra of DNA as a control; Fig. 6b represents the addition of DOX to DNA followed by DOC, denoted as DNA-DOX-DOC; Fig. 6c represents the addition of DOC before DOX, denoted as DNA-DOC-DOX; Fig. 6d represents the simultaneous addition of DOC and DOX,

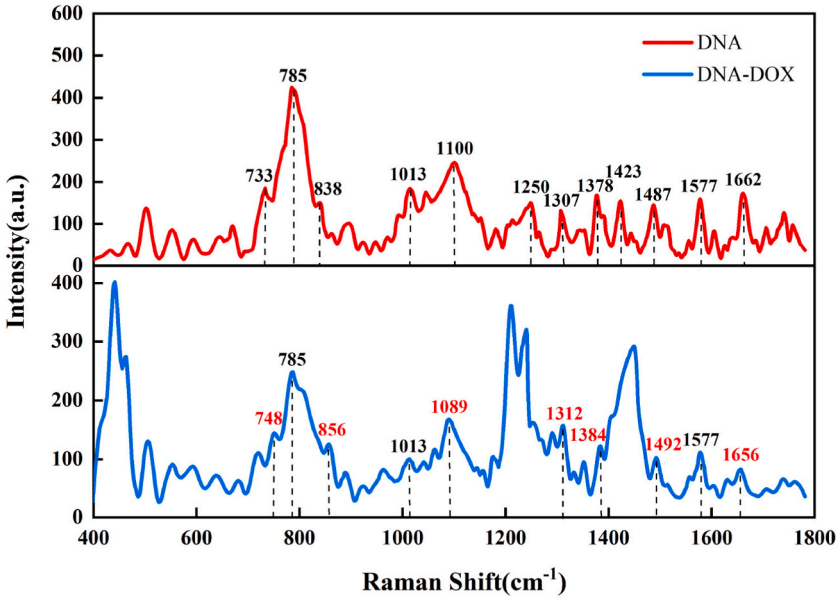

Fig. 5. Raman spectra of DNA and DNA-DOX solution.

denoted as DNA-(DOC-DOX).

Compared with DNA-DOX in Fig. 5, some of the Raman peaks of DNA in DNA-DOX-DOC significantly shifted in Fig. 6b. Raman peak corresponding to base A at 748 cm^{-1} shifted to 732 cm^{-1}, peak representing DNA conformation at 856 cm^{-1} shifted to 840 cm^{-1} and the peaks associated with bases A and G at 1492 and 1577 cm^{-1} shifted to 1484 and 1584 cm^{-1}. These shifts suggested that DOC can affect the intercalation of DOX, leading to changes in the degree of Raman peak shifts. In comparison with DNA-DOC in Fig. 3, the Raman peak of 740 cm^{-1} characterizing base A in DNA-DOC-DOX shifted to 730 cm^{-1} in Fig. 6c, while no significant change in other peak positions. This indicated that DOC can occupy some sites after interacting with DNA, resulting in fewer sites where DOX can interact.

Table 1 shows the peak positions and peak attribution when DOC and DOX interact with DNA in different sequences. Analyzing the shift degrees of the Raman peak in the ternary system, the shifts of 733 and 1307 cm^{-1} representing base A were within 2 cm^{-1}, indicating that the order of interaction had little effect on base A. The 838 cm^{-1} characteristic peak exhibited the maximum shift in DNA-DOC-DOX, with a shift of 7 cm^{-1}, indicating that the addition of DOC before DOX had the greatest effect on the DNA

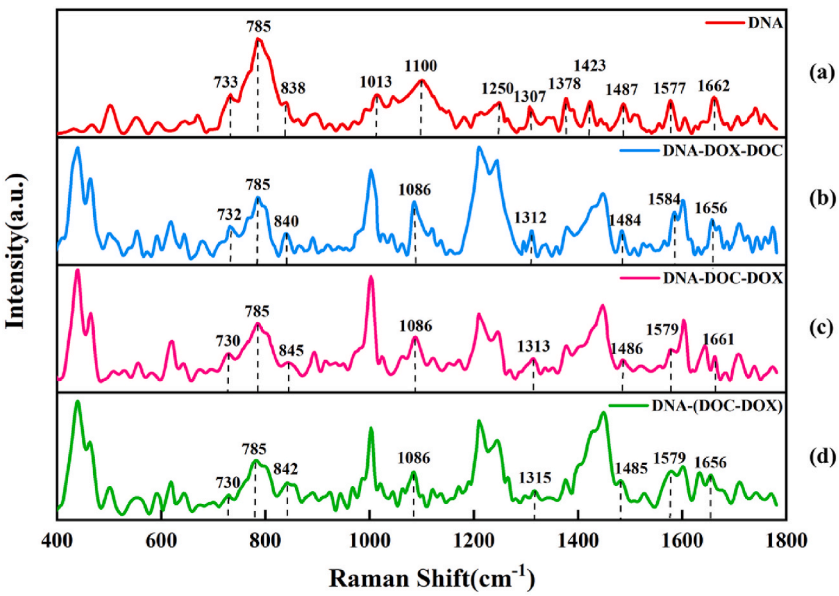

Fig. 6. Raman spectra of DNA, DOC and DOX complexes. (a) DNA; (b) DNA-DOX-DOC; (c) DNA-DOC-DOX; (d) DNA-(DOC-DOX).

conformation. The peaks associated with base G in DNA-DOX-DOC showed the maximum shift, with shifts of 3 and 7 cm^{-1} at 1487 and 1577 cm^{-1}, respectively. This indicated that interaction sequence of adding DOX first and then DOC had the strongest effect on base G, resulting in the most significant impact on DNA. The variation of 1662 cm^{-1} characterizing C═O was minimal in DNA-DOC-DOX, attributed to the partial occupancy of binding sites by the bacatine ring of DOC molecules after interacting with DNA, resulting in difficulty of insertion of DOX into DNA.

From the above analysis, it can be concluded that there exist synergistic effects and competitive relationships when DOC and DOX interact with DNA simultaneously. The different sequences of interaction of DOC and DOX with DNA not only affect the binding sites of drugs and DNA, but also cause changes in the environment surrounding the binding sites.

3.2. UV–vis spectra

The binding modes between drugs and DNA was further investigated by UV–vis spectroscopy. While the binding mode of DOX and DNA has been extensively studied [46,47], the following is a detailed study of the binding mode of DOC and DNA. The effects of pH, DNA concentration, interaction time, ionic strength and temperature on the UV–Vis spectra of DNA-DOC complexes were investigated. During the experiments, the concentration of DOX is 1.2×10^{-4} M, under the condition, the absorbance of DOX is about 0.6, and the measurement error will be relatively small. In order to avoid the influence of different concentrations of DOX and DOC, the concentration of DOC is also 1.2×10^{-4} M.

3.2.1. Effect of pH on DOC

Fig. 7 shows the UV–vis spectra of DOC at different pH in different wavelength ranges. Fig. 7a indicated that DOC had two absorption peaks at 190–260 nm, with peak I around 200 nm and peak II around 230 nm. As pH increasing, the intensity of peak I decreased significantly and the peak position was redshifted, while peak II had no significant change. Fig. 7b shows the UV–vis spectra of DOC at 220–300 nm. With the increase of pH, the intensity of DOC at 230 nm increased slightly and the peak position did not change significantly. The absorption peak at 230 nm was due to the π→π* transition of aromatic structure such as benzene ring. Additionally, there was also a weak absorption peak at 273 nm, attributed to the cycloalkyl groups in the DOC molecule and the methylene and epoxy groups on the stereoisomer. Therefore, due to the minimal impact of pH on the absorption peak at 230 nm, it is chosen as the standard for the qualitative identification and quantitative determination of DOC.

3.2.2. DNA concentration

Fig. 8 shows the UV–vis spectra of DNA-DOC. As shown in Fig. 8a, a hypochromic effect was observed in the DNA-DOC spectra with the increase of DNA concentration, and the hypochromic ratio was 25.35 %, indicating that DOC and DNA had a certain effect. This interaction may be attributed to the insertion of DOC into DNA, causing axial contraction and conformation change of DNA, leading to π-π* stacking and energy transition phenomena. An isosbestic point appeared around 244 nm, serving as a characteristic feature of intercalation [48,49]. Therefore, there may be intercalation between DOC and DNA, but the hypochromic effect was less than 40 %, and there was no significant blueshift or redshift, indicating differences from classical intercalation.

To further understand the binding strength between DOC and DNA, linear fitting with equation (1) was performed based on the UV–vis spectra at 230 nm in Fig. 8a and the results were presented in Fig. 8b.

$$\frac{1}{A - A_0} = \frac{1}{A} + \frac{1}{K_A \times A \times c_{DNA}} \tag{1}$$

Here, A_0 is the absorbance of free DOC at 230 nm, A is the absorbance at 230 nm at different DNA concentration, c_{DNA} is the concentration of DNA. The ratio of intercept 1/A to slope $1/(K_A \times A)$ can be used to calculate the binding constant K_A for the interaction between DOC and DNA and the result is $K_A = 5.25 \times 10^3$ M^{-1}. In comparison, the binding constant of the interaction between DOX and DNA is 6.50×10^4 M^{-1} [50]. Therefore, the binding between DOX and DNA is more stable than that between DOC and DNA.

3.2.3. Interaction time

Fig. 9 shows the UV–vis spectra of DNA-DOC complex at different times. The absorbance at 230 nm of DNA-DOC showed no significant changes, with only a slight fluctuation of approximately 0.04 nm, indicating good stability of DNA-DOC complex.

Table 1
Location and attribution of DNA, DOC and DOX complexes (400–1800 cm^{-1}).

DNA	DNA-DOX-DOC	DNA-DOC-DOX	DNA-(DOC-DOX)	Attribution
733	732	730	730	A
838	840	845	842	B-DNA
1100	1086	1086	1086	O═P═O
1307	1312	1313	1315	A
1487	1484	1486	1485	G、A
1577	1584	1579	1579	T、A、G
1662	1656	1661	1656	C═O

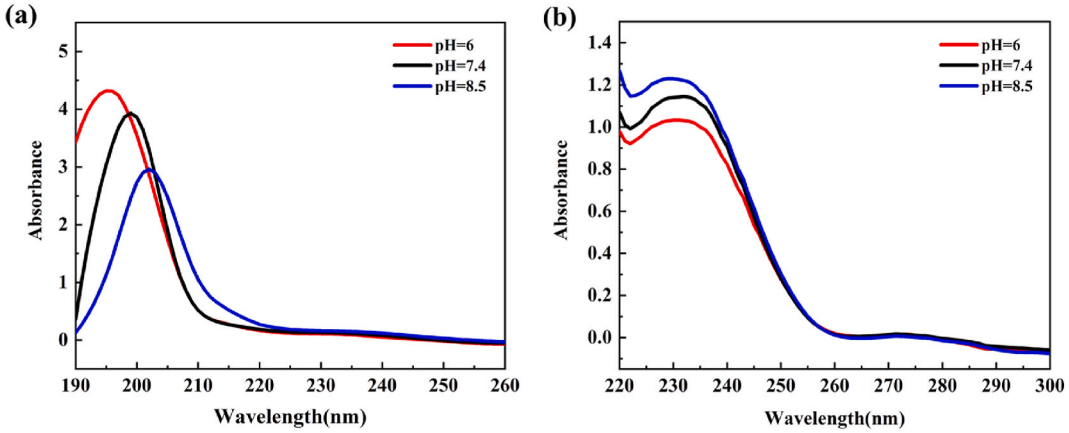

Fig. 7. UV–vis spectra of DOC in different wavelength ranges (pH = 6、7.4、8.5). (a) 190–260 nm; (b) 220–300 nm.

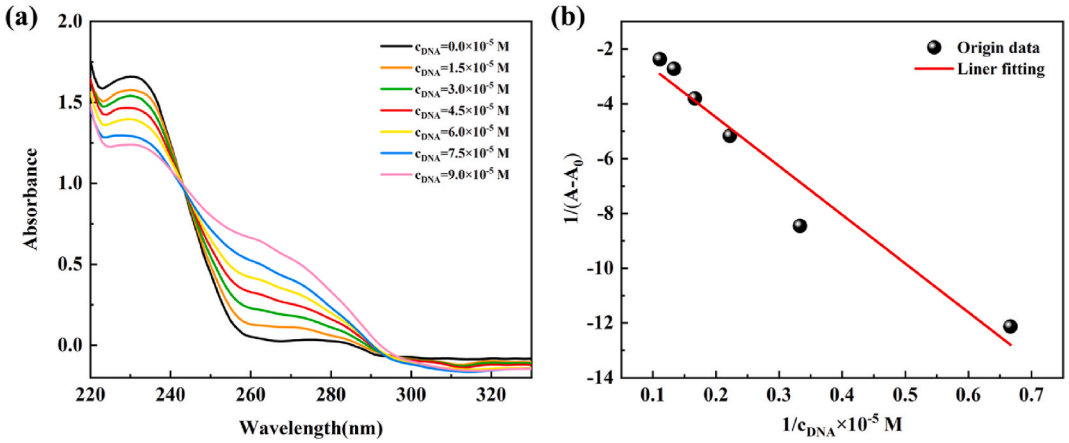

Fig. 8. UV–vis spectra of DNA-DOC. (a) UV–vis spectra of DOC (1.2×10^{-4} M) in the presence of increasing concentration of DNA (0–9.0×10^{-5} M) in Tris-HCl buffer (pH = 7.4); (b) linear variation of $1/(A\text{-}A_0)$ and 1/[DNA].

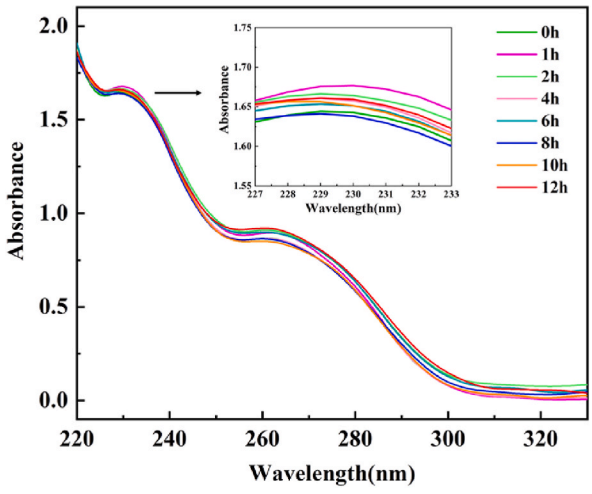

Fig. 9. UV–vis absorption spectra of DNA-DOC at different times, c(DNA) = 1.5×10^{-4} M, c(DOC) = 1.2×10^{-4} M.

3.2.4. Melting point experiment

The thermal melting temperature (T_m) is the temperature at which the DNA double helix structure is decomposed into half, and it is also one of the indexes to judge the stability of DNA molecular structure [51].To further verify the stability of DNA-DOC, the T_m of the complex was investigated in the experiment. The thermal denaturation curves of DNA and DNA-DOC solution were prepared according to equation (2):

$$f_{ss} = \frac{A - A_0}{A_f - A_0} \tag{2}$$

In the equation, f_{ss} represents the unwinding degree of DNA, A is the absorbance of DNA (or DNA-DOC) at 260 nm at different temperatures, A_0 and A_f represent the initial and final absorbance.

Fig. 10 shows the thermal denaturation curve of DNA and DNA-DOC. The T_m of DNA and DNA-DOC are 77.56 °C and 82.63 °C, respectively. The double helix structure of DNA has a significant stability under the effect of hydrogen bonding and base stacking. When the temperature increases, the binding force weakens and the DNA double helix dissociates into single strands [52]. Intercalation can enhance the stability of the DNA double helix structure, increasing T_m by approximately 5–8 °C [53]. After interacting with DOC, the T_m of DNA increased by 5.07 °C. This indicated that DNA-DOC had a strong stability and further confirmed the intercalation between DOC and DNA.

3.2.5. Ionic strength

Electrostatic binding is a non-covalent mode of small molecules interacting with DNA and is generally considered as an auxiliary mode of groove and intercalation [54]. To explore whether electrostatic binding plays a role in the interaction between DOC and DNA, ionic strength experiment was performed.

Fig. 11 illustrates the absorbance change trend of DNA-DOC solution at 230 nm under different NaCl concentration. With the increase of NaCl concentration, the absorbance of the spectra increased slightly. This is attributed to the binding of positively charged Na^+ and negatively charged phosphate backbone, reducing the repulsion between two DNA strands [55], which weakens the intercalation between DOC and DNA molecules. Ionic strength experiment suggests an electrostatic binding between DOC and DNA.

3.2.6. UV–vis spectra of DNA, DOC and DOX complexes

Fig. 12 illustrates the UV–vis spectra of DNA, DOC and DOX complexes. Table 2 shows the peak intensity, absorption peak position, peak shift and hypochromic ratio of UV–vis spectra of the ternary system. As depicted in Fig. 12, it can be seen that the spectrum of DOX-DOC hardly changes comparing to the spectrum of DOX. Therefore, the effect of the interaction between DOX and DOC can be neglected. A significant redshift and hypochromic phenomenon were observed after the interaction of DNA and DOX, with a 7 nm redshift and 42.6 % hypochromic ratio. This is due to the insertion of DOX into DNA to form a stable complex. The hypochromic ratio of DNA-DOX-DOC was 37.8 %, suggesting that DOC can affect the insertion of DOX into DNA, indicating the competitive relationships between DOC and DOX.

Compared to the ternary system, the absorption peak of DNA-DOC-DOX was redshifted by 2 nm and the hypochromic ratio was 4.1 %. This small redshift and hypochromic degree are attributed to DOC occupying some sites after interacting with DNA, resulting in fewer insertion sites of DOX. However, the absorption peak of DNA-(DOC-DOX) was redshifted by 3 nm and the hypochromic ratio was 19.9 %. This is due to the entanglement of the long chain of DOC on the DOX molecule to prevent part of DOX from inserting into the DNA, resulting in less redshift and hypochromic degree.

Since the different interaction orders of DOC and DOX with DNA in the UV–vis spectra of the ternary system would result in redshift

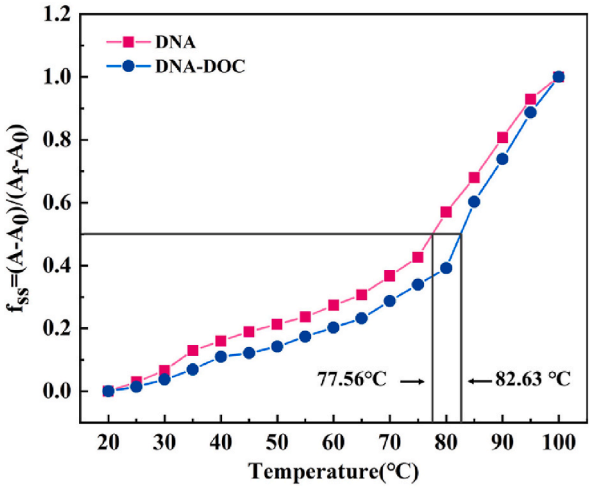

Fig. 10. Thermal melting curves of DNA in the absence and presence of Docetaxel, c(DNA) = 1.5×10^{-4} M, c(DOC) = 1.2×10^{-4} M.

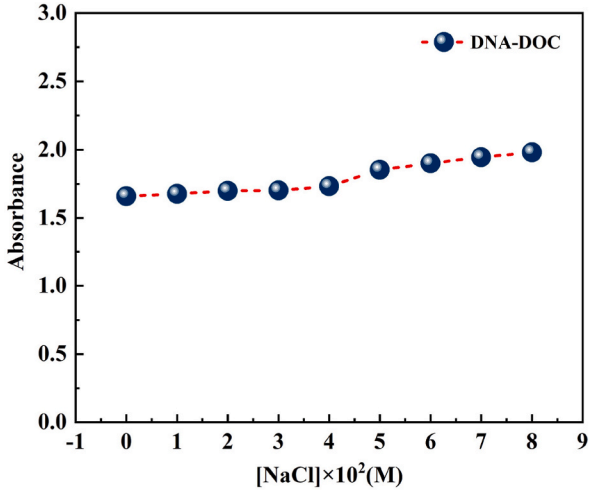

Fig. 11. Effect of NaCl concentration on UV–vis spectra of DNA-DOC, c(DNA) = 1.5 × 10^{-4} M, c(DOC) = 1.2 × 10^{-4} M, c(NaCl) = 1.0–8.0 × 10^{-2} M.

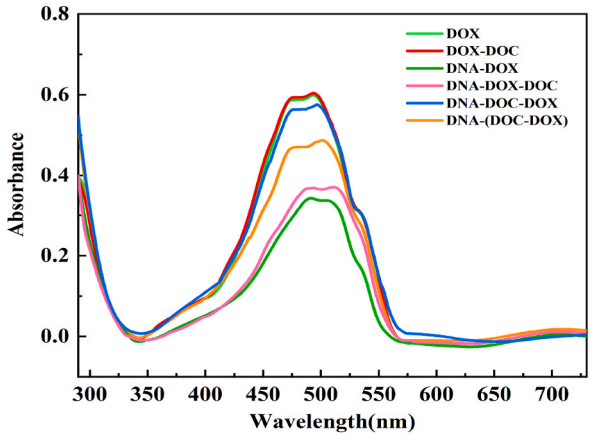

Fig. 12. UV–vis spectra of DNA, DOC and DOX complexes.

Table 2
UV–vis spectra peak position changes of the ternary system.

	Intensity	Absorption peak (nm)	Shift (nm)	Hypochromic ratio
DOX	**0.587**	**484**	**0**	**0**
DNA-DOX	**0.337**	**501**	**7**	**42.6 %**
DNA-DOX-DOC	**0.365**	**501**	**7**	**37.8 %**
DNA-DOC-DOX	**0.563**	**486**	**2**	**4.1 %**
DNA-(DOC-DOX)	**0.470**	**487**	**3**	**19.9 %**

and hypochromicity, indicating a synergistic interaction between DOC and DOX. However, due to the different orders of interaction, the degree of redshift and hypochromicity was different, indicating the competition relationships between DOC and DOX.

3.3. Molecular docking results

The molecular docking results of DOC and DOX with DNA are shown in Fig. 13 and Fig. 14. The docking binding energy of DOC and DNA is −5.71 kcal/mol and the intermolecular energy (including van der Waals forces, hydrogen bonds, desolvation energy and electrostatic energy) was −10.78 kcal/mol. Figs. 13a–c shows that the C13 side chain of DOC inserted into DNA. The oxygen atom (O) in the side chain forms a hydrogen bond with the nitrogen atom (N) of base G and the hydroxyl group (-OH) forms a hydrogen bond with the amino sugar group (-NH_2) of base G, with length of 1.9 Å and 2.2 Å. The O atom of DOC bacatine ring forms a hydrogen bond

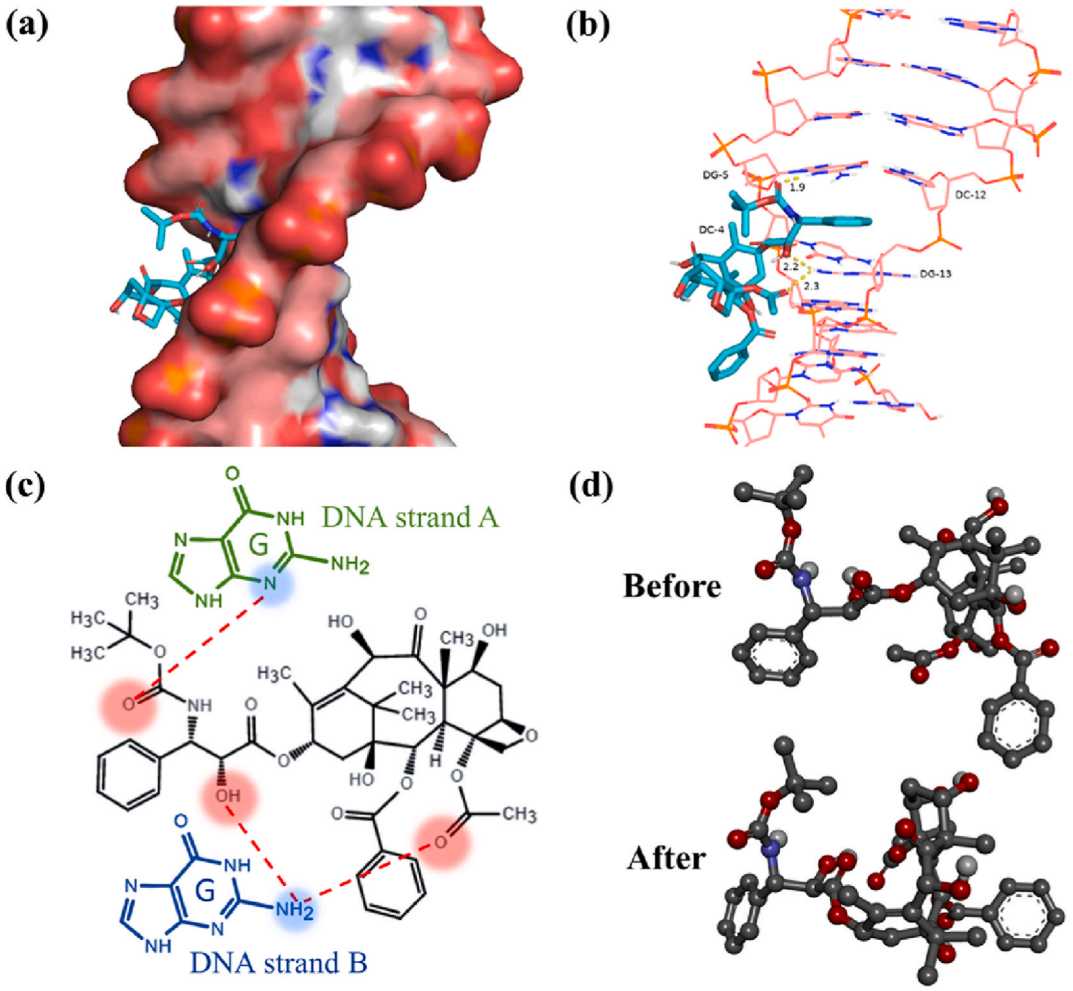

Fig. 13. Molecular docking results of interaction between DOC and DNA. (a) Binding mode; (b) Hydrogen bond length; (c) Interaction sites; (d) Conformation of free DOC and DOC after interacting with DNA.

of 2.3 Å with –NH_2 of base G, stabilizing the molecule in the groove and helping the phenyl group to insert into the DNA. Fig. 13d shows the conformation of free DOC and DOC after interacting with DNA. The C13 side chain of DOC is twisted, resulting in a change in conformation, implying the role of flexibility in stabilizing the DNA-DOC complex. The docking results indicate that hydrogen bonds play an important role in the binding of DOC and DNA.

The docking binding energy of DOX and DNA is −9.38 kcal/mol and the intermolecular energy (including van der Waals forces, hydrogen bonds, desolvation energy and electrostatic energy) was −12.66 kcal/mol. Figs. 14a–c shows that the tetracyclic ring of DOX is inserted into the base pairs. The –OH at C9 forms a hydrogen bond with the N atom of base G and the O atom at C7 forms a hydrogen bond with –NH_2 of base G, with length of 1.9 Å and 1.8 Å. The –NH_2 of DOX forms a hydrogen bond of 2.2 Å with the O atom of base C in the minor groove of DNA. Fig. 14d shows the conformation of free DOX and DOX after interacting with DNA, the amino sugar group is twisted to affect its conformation.

The molecular docking results show that both DOC and DOX can insert into the base pairs of DNA and form hydrogen bonds with the 2 and 3 sites of base G. When DOC and DOX interact together on DNA molecules, the –OH at C9 of DOX competes with the O atom of the DOC side chain, while the O atom at C7 of DOX competes with the –OH of DOC. The binding of DNA and DOX is more stable than that of DOC due to the lower binding energy between DNA and DOX.

3.4. The interaction mechanism of DOC and DOX with DNA

Fig. 15 illustrates the interaction mechanism of DOC and DOX with DNA. When DNA interacts with DOX, DOX inserts into base pairs and binds to DNA through hydrogen bonds and electrostatic interaction. When DOC subsequently interacts with DNA, DOC may interact with other sites of DNA or displace a small amount of DOX molecules. When DNA interacts with DOC, the side chain of DOC inserts into DNA and its bacatine ring forms hydrogen bonds with DNA in the groove. This occupies part of potential binding sites of

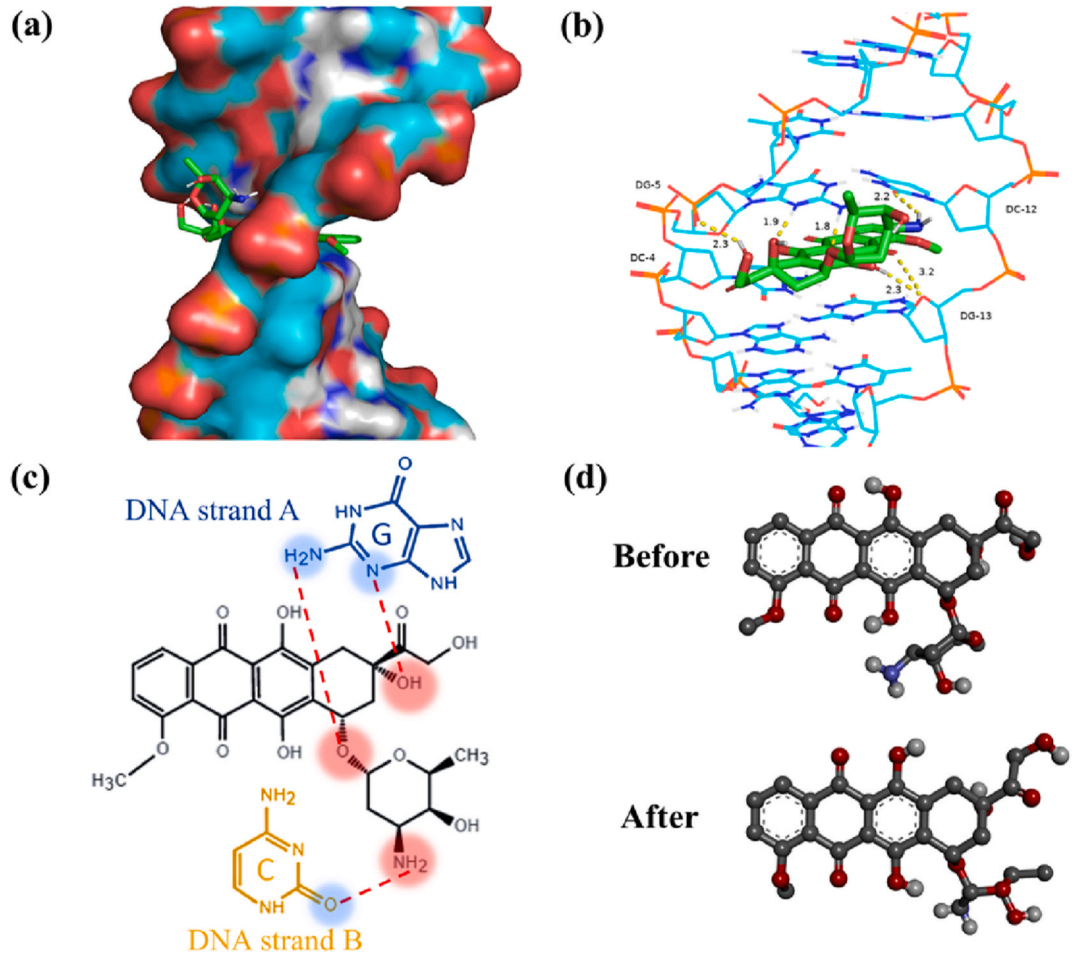

Fig. 14. Molecular docking results of interaction between DOX and DNA. (a) Binding mode; (b) Hydrogen bond length; (c) Interaction sites; (d) Conformation of free DOX and DOX after interacting with DNA.

DOX and DNA, making it difficult for DOX to insert into DNA. When both DOC and DOX interact with DNA simultaneously, the long chain of DOC molecules will wrap around some DOX molecules, resulting in some DOC and DOX remain free in solution and the rest DOC and DOX molecules interact with DNA by hydrogen bonds and electrostatic interaction.

4. Conclusion

In this study, laser confocal Raman spectroscopy, UV–vis spectroscopy and molecular docking technology were used to investigate the interaction mechanism between DOC and DNA molecules, as well as the synergistic effects and competitive relationships between DOC and DOX as acting on DNA molecules. The results of Raman spectroscopy showed some meaningful results. When DOC or DOX interacts alone with DNA molecules, Raman peaks of DNA have different degree shifts, indicating both DOC and DOX can interact with bases and phosphate backbone of DNA molecules, and also lead to DNA conformation changes. When DOC and DOX act on DNA molecules simultaneously, the effect is different from that of single drug. Moreover, the different orders of DOC and DOX acting on DNA molecules lead to different changes of DNA Raman peak positions, that is, the binding sites between drugs and DNA are affected. The order of DOX acting firstly and then DOC has a greater effect on base G, and the effect is more stable, which shows the high efficiency of the clinical treatment scheme of using anthracycline drugs first and then taxanes to some extent. UV–vis absorption spectroscopy was used to systematically investigate the effects of DNA concentration, ionic strength, interaction time and temperature on DNA-DOC, the experiment results indicated that the interaction modes between DOC and DNA are non-classical intercalation binding and electrostatic binding. Molecular docking results showed that the C13 side chain of DOC molecule can insert into DNA molecule and form hydrogen bonds with base G, confirming the correlation between C13 side chain and anticancer activity. The difference in binding energy between DNA-DOC and DNA-DOX indicated the basis of better effectiveness in clinical treatment using DOX firstly and then DOC. The research results of this study elucidate the interaction mechanism of DNA-DOC, as well as the synergistic effects and competitive relationships between DOC and DOX as acting on DNA molecules at the single-molecule level. This study provides a theoretical foundation for designing and developing less toxic antitumor drugs and drug combination therapy for

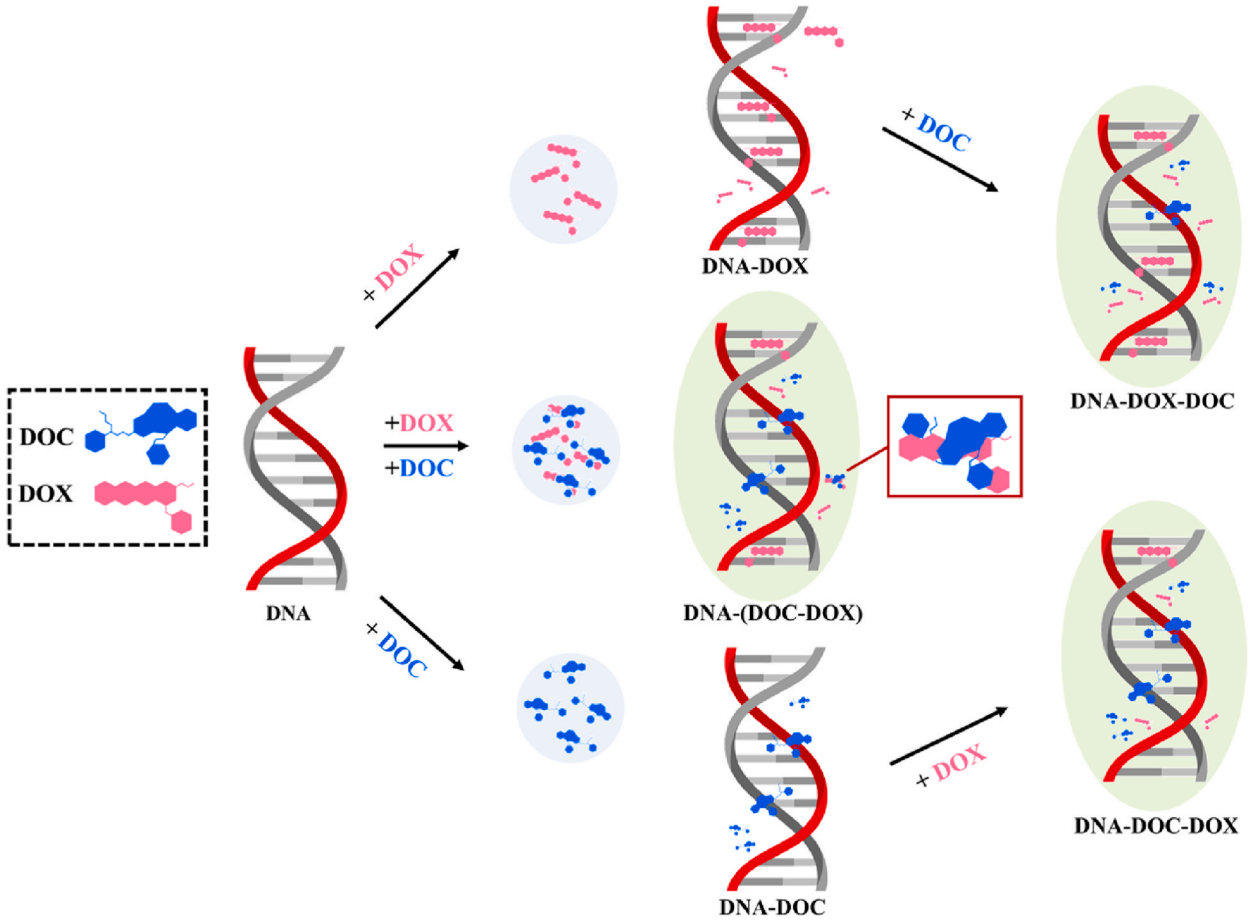

Fig. 15. The interaction mechanism of DOC and DOX with DNA.

cancer.

CRediT authorship contribution statement

Suli Zhou: Writing – original draft, Visualization, Software, Formal analysis, Data curation. **Xiaoqiang Feng:** Supervision, Methodology, Conceptualization. **Jintao Bai:** Supervision, Project administration. **Dan Sun:** Supervision, Methodology. **Baoli Yao:** Writing – review & editing, Supervision. **Kaige Wang:** Writing – review & editing, Supervision, Project administration, Methodology, Conceptualization.

Declaration of competing interest

The authors declare that they have no known competing financial interests or personal relationships that could have appeared to influence the work reported in this paper.

Acknowledgments

This work was supported by the National Natural Science Foundation of China (Grant numbers 62275216, 61775181); the Innovation Capability Support Program of Shaanxi Province (Grant No. S2018-ZC-TD-0061, TZ0393); the National Key Scientific Instrument and Equipment Development Projects of China (No. 51927804); and the State Key Laboratory of Transient Optics and Photonics, Chinese Academy of Sciences (SKLST202109).

References

[1] Y.N. Xiong, J.S. Li, G.X. Huang, L.J. Yan, J. Ma, Interacting mechanism of benzo (a) pyrene with free DNA in vitro, Int. J. Biol. Macromol. 167 (2021) 854–861.
[2] J.B. Chaires, Drug—DNA interactions, Curr. Opin. Struct. Biol. 8 (1998) 314–320.

[3] Y.T. Sun, S.Y. Bi, D.Q. Song, C.Y. Qiao, D. Mu, H.Q. Zhang, Study on the interaction mechanism between DNA and the main active components in Scutellaria baicalensis Georgi, Sens. Actuator B-Chem. 129 (2008) 799–810.
[4] D.E. Gilbert, J. Feigon, Structural analysis of drug-DNA interactions, Curr. Opin. Struct. Biol. 1 (1991) 439–445.
[5] G. Bischoff, S. Hoffmann, DNA-binding of drugs used in medicinal therapies, Curr. Med. Chem. 9 (2002) 321–348.
[6] M. Rizzo, Mechanisms of docetaxel resistance in prostate cancer: the key role played by miRNAs, Biochim. Biophys. Acta-Rev. Cancer 1875 (2021) 188481.
[7] M. Imran, S. Saleem, A. Chaudhuri, J. Ali, S. Baboota, Docetaxel: an update on its molecular mechanisms, therapeutic trajectory and nanotechnology in the treatment of breast, lung and prostate cancer, J. Drug Deliv. Sci. Technol. 60 (2020) 101959.
[8] M.A. Jordan, L. Wilson, Microtubules as a target for anticancer drugs, Nat. Rev. Cancer 4 (2004) 253–265.
[9] Q. Tan, X.J. Liu, X.Y. Fu, Q.L. Li, J.F. Dou, G.X. Zhai, Current development in nanoformulations of docetaxel, Expert Opin. Drug Deliv. 9 (2012) 975–990.
[10] N.A. Alsaif, A.A. Al-Mehizia, A.H. Bakheit, S. Zargar, T.A. Wani, A spectroscopic, thermodynamic and molecular docking study of the binding mechanism of dapoxetine with calf thymus DNA, S. Afr. J. Chem. 73 (2020) 44–50.
[11] S. Ponkarpagam, G. Mahalakshmi, K.N. Vennila, K.P. Elango, Multi-spectroscopic, voltammetric and molecular docking studies on binding of anti-diabetic drug rosigiltazone with DNA, Spectroc. Acta Pt. A-Molec. Biomolec. Spectr. 234 (2020) 118268.
[12] M. Dareini, Z.A. Tehranizadeh, N. Marjani, R. Taheri, S. Aslani-Firoozabadi, A. Talebi, N.N. Eidgahi, M.R. Saberi, J. Chamani, A novel view of the separate and simultaneous binding effects of docetaxel and anastrozole with calf thymus DNA: experimental and in silico approaches, Spectroc. Acta Pt. A-Molec. Biomolec. Spectr. 228 (2020) 117528.
[13] D. Kreft, Y. Wang, M. Rattay, K. Toensing, D. Anselmetti, Binding mechanism of anti-cancer chemotherapeutic drug mitoxantrone to DNA characterized by magnetic tweezers, J. Nanobiotechnol. 16 (2018) 1–7.
[14] E.A. Costa, A.P. Gonçalves, J.A.D. Batista, R.F. Bazoni, A.A. Santos, M.S. Rocha, New insights into the mechanism of action of the drug chloroquine: direct interaction with DNA and cytotoxicity, J. Phys. Chem. B 126 (2022) 3512–3521.
[15] P.R. Ipte, A. Sharma, H. Pal, A.K. Satpati, Probing the interaction of ciprofloxacin with dsDNA: electrochemical, spectro-electrochemical and AFM investigation, J. Electroanal. Chem. 885 (2021) 115098.
[16] K. Klein, A.M. Gigler, T. Aschenbrenner, R. Monetti, W. Bunk, F. Jamitzky, G. Morfill, R.W. Stark, J. Schlegel, Label-free live-cell imaging with confocal Raman microscopy, Biophys. J. 102 (2012) 360–368.
[17] G.J. Myres, E.M. Peterson, J.M. Harris, Confocal Raman microscopy enables label-free, quantitative, and structurally informative detection of DNA hybridization at porous silica surfaces, Anal. Chem. 93 (2021) 7978–7986.
[18] S. Rezaei, H.S. Meftah, Y. Ebtehajpour, H.R. Rahimi, J. Chamani, Investigation on the effect of fluorescence quenching of calf thymus DNA by piperine: caspase activation in the human breast cancer cell line studies, DNA Cell Biol. 43 (2024) 26–38.
[19] Z. Malek-Esfandiari, A. Rezvani-Noghani, T. Sohrabi, P. Mokaberi, Z. Amiri-Tehranizadeh, J. Chamani, Molecular dynamics and multi-spectroscopic of the interaction behavior between bladder cancer cells and calf thymus DNA with rebeccamycin: apoptosis through the down regulation of PI3K/AKT signaling pathway, J. Fluoresc. 33 (2023) 1537–1557.
[20] F.D. Sani, N. Shakibapour, S. Beigoli, H. Sadeghian, M. Hosainzadeh, J. Chamani, Changes in binding affinity between ofloxacin and calf thymus DNA in the presence of histone H1: spectroscopic and molecular modeling investigations, J. Lumin. 203 (2018) 599–608.
[21] Early Breast Cancer Trialists' Collaborative Group, Anthracycline-containing and taxane-containing chemotherapy for early-stage operable breast cancer: a patient-level meta-analysis of 100 000 women from 86 randomised trials, Lancet 401 (2023) 1277–1292.
[22] N. Shao, S.M. Wang, C. Yao, X.D. Xu, Y.J. Zhang, Y.Y. Zhang, Y. Lin, Sequential versus concurrent anthracyclines and taxanes as adjuvant chemotherapy of early breast cancer: a meta-analysis of phase III randomized control trials, Breast 21 (2012) 389–393.
[23] M. Zaheed, N. Wilcken, M.L. Willson, D.L. O'Connell, A. Goodwin, Sequencing of anthracyclines and taxanes in neoadjuvant and adjuvant therapy for early breast cancer, Cochrane Database Syst. Rev. 2 (2019) 1465–1858.
[24] S. Roy, S. Lakritz S, A.R. Schreiber, E. Molina, P. Kabos, M. Wood, A. Elias, L. Kondapalli, C.J. Bradley, J.R. Diamond, Clinical outcomes of adjuvant taxane plus anthracycline versus taxane-based chemotherapy regimens in older adults with node-positive, triple-negative breast cancer: a SEER–Medicare study, Eur. J. Cancer 185 (2023) 69–82.
[25] G. Bonadonna, S. Monfardini, M.D. Lena, F. Fossati-Bellani, Clinical evaluation of adriamycin, a new antitumour antibiotic, Br. Med. J. 3 (1969) 503–506.
[26] S.S. Tartakoff, J.M. Finan, E.J. Curtis, H.M. Anchukaitis, D.J. Couture, S. Glazier, Investigations into the DNA-binding mode of doxorubicinone, Org. Biomol. Chem. 17 (2019) 1992–1998.
[27] S. Rivankar, An overview of doxorubicin formulations in cancer therapy, J. Canc. Res. Ther 10 (2014) 853–858.
[28] L. Trynda-Lemiesz, M. Łuczkowski, Human serum albumin: spectroscopic studies of the paclitaxel binding and proximity relationships with cisplatin and Adriamycin, J. Inorg. Biochem. 98 (2004) 1851–1856.
[29] Z.G. Chen, S.H. Qian, X. Chen, J.H. Chen, G.M. Zhang, G.H. Zeng, Investigation on the interaction between anthracyclines and DNA in the presence of paclitaxel by resonance light scattering technique, Microchim. Acta 177 (2012) 67–73.
[30] S. Zeng, Y.Z. Chen, L.W. Fu, K.R. Johnson, W.M. Fan, In vitro evaluation of schedule-dependent interactions between docetaxel and doxorubicin against human breast and ovarian cancer cells, Clin. Cancer Res. 6 (2000) 3766–3773.
[31] F. Kheirdoosh, M. Pazhavand, M. Sariaslani, N.H. Moghadam, S. Salehzadeh, Multi-spectroscopic and molecular docking studies on the interaction of neotame with calf thymus DNA, Nucleosides Nucleotides Nucleic Acids 39 (2020) 699–714.
[32] T.A. Wani, N. Alsaif, A.H. Bakheit, S. Zargar, A.A. Al-Mehizia, A.A. Khan, Interaction of an abiraterone with calf thymus DNA: investigation with spectroscopic technique and modelling studies, Bioorganic Chem 100 (2020) 103957.
[33] G.K. Wang, C.L. Yan, D.C. Wang, D. Li, Y. Lu, Specific binding of a dihydropyrimidinone derivative with DNA: spectroscopic, calorimetric and modeling investigations, J. Lumin. 132 (2012) 1656–1662.
[34] B. Prescott, W. Steinmetz, G.J. Thomas, Characterization of DNA structures by laser Raman spectroscopy, Biopolymers 23 (1984) 235–256.
[35] L.N. Yao, Y.J. Li, Z.Z. Zuo, Z.Y. Gong, J. Zhu, X.Q. Feng, D. Sun, K.G. Wang, Studying the interaction between bendamustine and DNA molecule with SERS based on AuNPs/ZnCl2/NpAA solid-state substrate, Int. J. Mol. Sci. 24 (2023) 13517.
[36] D.C. Goodwin, J. Brahms, Form of DNA and the nature of interactions with proteins in chromatin, Nucleic Acids Res. 5 (1978) 835–850.
[37] S.P.A. Fodor, P.A. Starr, T.G. Spiro, Raman spectroscopic elucidation of DNA backbone conformations for poly(dG-dT) • poly(dA-dC) and poly(dA-dT) • poly (dA-dT) in CsF solution, Biopolymers 24 (1985) 1493–1500.
[38] P. Cipriani, D. Ben-Amotz, Characterization of select members of the taxane family using Raman spectroscopy, J. Raman Spectrosc. 36 (2005) 1052–1058.
[39] M.C.O. da Rocha, P.B. da Silva, M.A. Radicchi, B.Y.G. Andrade, J.V. de Oliveira, T. Venus, C. Merker, I. Estrela-Lopis, J.P.F. Longo, S.N. Báo, Docetaxel-loaded solid lipid nanoparticles prevent tumor growth and lung metastasis of 4T1 murine mammary carcinoma cells, J. Nanobiotechnol. 18 (2020) 1–20.
[40] H.J. Byrne, F. Bonnier, Z. Farhane, Two-dimensional correlation analysis of Raman microspectroscopy of subcellular interactions of drugs in vitro, J. Biophot. 12 (2019) e201800328.
[41] F. Bonnier Farhane, O. Howe, A. Casey, H.J. Byrne, Doxorubicin kinetics and effects on lung cancer cell lines using in vitro Raman micro-spectroscopy: binding signatures, drug resistance and DNA repair, J. Biophot. 11 (2018) e201700060.
[42] E. Szafraniec, K. Majzner, Z. Farhane, H.J. Byrne, M. Lukawska, I. Oszczapowicz, S. Chlopicki, M. Baranska, Spectroscopic studies of anthracyclines: structural characterization and in vitro tracking, Spectroc. Acta Pt. A-Molec. Biomolec. Spectr. 169 (2016) 152–160.
[43] Z. Farhane, F. Bonnier, M.A. Maher, J. Bryant, A. Casey, H.J. Byrne, Differentiating responses of lung cancer cell lines to Doxorubicin exposure: in vitro Raman micro spectroscopy, oxidative stress and bcl-2 protein expression, J. Biophot. 10 (2017) 151–165.
[44] M. Manfait, A.J.P. Alix, P. Jeannesson, J.C. Jardillier, T. Theophanides, Interaction of adriamycin with DNA as studied by resonance Raman spectroscopy, Nucleic Acids Res. 10 (1982) 3803–3816.
[45] C.J. Lee, J.S. Kang, M.S. Kim, K.P. Lee, M.S. Lee, The study of doxorubicin and its complex with DNA by SERS and UV-resonance Raman spectroscopy, Bull. Korean Chem. Soc. 25 (2004) 1211–1216.

[46] X.Z. Zhang, A. Poniewierski, K. Sozański, Y. Zhou, A. Brzozowska-Elliott, R. Holyst, Fluorescence correlation spectroscopy for multiple-site equilibrium binding: a case of doxorubicin-DNA interaction, Phys. Chem. Chem. Phys. 21 (2019) 1572–1577.
[47] R.H. Zhang, J. Zhu, D. Sun, J. Li, L.N. Yao, S.S. Meng, Y. Li, Y. Dang, K.G. Wang, The mechanism of dynamic interaction between doxorubicin and calf thymus DNA at the single-molecule level based on confocal Raman spectroscopy, Micromachines 13 (2022) 940.
[48] N.K. Modukuru, K.J. Snow, B.S. Perrin, J. Thota, C.V. Kumar, Contributions of a long side chain to the binding affinity of an anthracene derivative to DNA, J. Phys. Chem. B 109 (2005) 11810–11818.
[49] S.I. Farooqi, N. Arshad, P.A. Channar, F. Perveen, A. Saeed, F.A. Larik, A. Javeed, Synthesis, theoretical, spectroscopic and electrochemical DNA binding investigations of 1, 3, 4-thiadiazole derivatives of ibuprofen and ciprofloxacin: cancer cell line studies, J. Photochem. Photobiol. B Biol. 189 (2018) 104–118.
[50] W. Huan, X.X. Gou, X.H. Pu, J. Wang, X.B. Hu, Z.X. Li, Exploration of the interaction mechanism between Doxorubicin hydrochloride and DNA by spectroscopic techniques and isothermal titration calorimetry, Spectrosc. Spectr. Anal. 38 (2018) 540–545.
[51] S. Afrin, Y. Rahman, T. Sarwar, M.A. Husain, A. AliShamsuzzaman, M. Tabish, Molecular spectroscopic and thermodynamic studies on the interaction of anti-platelet drug ticlopidine with calf thymus DNA, Spectroc. Acta Pt. A-Molec. Biomolec. Spectr. 186 (2017) 66–75.
[52] M.F. Alam, S. Varshney, M.A. Khan, A.A. Laskar, H. Younus, In vitro DNA binding studies of therapeutic and prophylactic drug citral, Int. J. Biol. Macromol. 113 (2018) 300–308.
[53] B.J. Shen, H.R. Yang, J.Q. Chen, X.Y. Liu, M.Y. Zhou, Study the interaction between juglone and calf thymus DNA by spectroscopic and molecular docking techniques, Spectroc. Acta Pt. A-Molec. Biomolec. Spectr. 261 (2021) 119998.
[54] Y.T. Lei, Z.H. Zhang, X.L. Ma, R.R. Cai, L.L. Dai, Y. Guo, X. Tuo, Deciphering the interaction of perampanel and calf thymus DNA: a multi-spectroscopic and computer modelling study, J. Mol. Struct. 1270 (2022) 133900.
[55] S.B. Kou, K.L. Zhou, Z.Y. Lin, Y.Y. Lou, J.H. Shi, Y.X. Liu, Insights into the binding properties of calf thymus DNA with lopinavir from spectroscopic and computational studies, J. Mol. Liq. 328 (2021) 115491.